International Journal of Fluid Machinery and Systems
Vol. 7, No. 3, July-September 2014

DOI: http://dx.doi.org/10.5293/IJFMS.2014.7.3.094
ISSN (Online): 1882-9554

Original Paper (Invited)

Study of Cavitation Instabilities in Double-Suction Centrifugal Pump

Shinya Hatano[1], Donghyuk Kang[1], Shusaku Kagawa[2], Motohiko Nohmi[2]and Kazuhiko Yokota[1]

[1]Mechanical Engineering, Aoyama Gakuin University
Fuchinobe 5-10-1, Chuou-ku, Sagamihara, Kanagawa 252-5258, Japan,
c5613129@aoyama.jp, kang@me.aoyama.ac.jp, yokota@me.aoyama.ac.jp
[2]Fluid Machinery & Systems Company, EBARA Corporation,
Shintomi 78-1, Futtsu-shi, Chiba 293-0011, Japan
kagawa.shusaku@ebara.com, nohmi.motohiko@ebara.com

Abstract

In double-suction centrifugal pumps, it was found that cavitation instabilities occur with vibration and a perio dic chugging noise. The present study attempts to identify cavitation instabilities in the double-suction centrifugal pump by the experiment and Computational Fluid Dynamics (CFD). Cavitation instabilities in the tested pump were classified into three types of instabilities. The first one, in a range of cavitation number higher than breakdown cavitation number, is cavitation surge with a violent pressure oscillation. The second one, in a range of cavitation number higher than the cavitation number of cavitation surge, is considered to be rotating cavitation and causes the pressure oscillation due to the interaction of rotating cavitation with the impeller. Last one, in a range of cavitation number higher than the cavitation number of rotating cavitation, is considered to be a surge type instability.

Keywords: Double-suction centrifugal pump, Cavitation instability, Interaction of rotating cavitation with the impeller

1. Introduction

With the increased rotational speed for high performance and miniaturization, cavitation occurs easily in just upstream of an impeller and causes severe shaft vibration, noise and pressure breakdown. In high-speed pumps, it has been reported that the fluctuating phenomena occur at a low inlet pressure and a certain flow rate. These phenomena are called cavitation instabilities and have been mainly researched in axial pumps for rocket engines [1, 2, 3]. In the other hand, the researches for cavitation instabilities in centrifugal pumps have been rarely reported [4,5].

The authors observed cavitation instabilities with vibration and a periodic chugging noise in a double-suction centrifugal pump. The present study attempts to identify cavitation instabilities in the double-suction centrifugal pump by the experiment and Computational Fluid Dynamics (CFD).

2. Experimental and Computational Methods

2.1 Experimental Method

Figure 1 shows the schematic of test facilities and a tested pump. All lengths are normalized by the diameter of impeller D. The cavitation tunnel is a closed type and the inlet pressure is adjusted by controlling the tank pressure with a vacuum pump and a relief valve. The flow rate is controlled by the butterfly valve installed downstream of the tested pump. The impeller is driven by an inverter motor. The working fluid is a water. The flow coefficient $\phi=v/U$ and the cavitation number $\sigma=(p_3-p_v)/(\rho U^2/2)$ are used as test parameters in the present study. Here, v and U are the mean axial velocity at the suction pipe ③ and the tip speed of the impeller, respectively. p_v and p_3 are the vapor pressure and the inlet pressure at the suction pipe ③, respectively. ρ is the density of the working fluid. The flow rate and the pressures were measured by a venturi meter and pressure transducers of a strain-gage type, respectively. During the operation of the tested pump, the flow rate, the pressures, the torque, the water temperature and the rotational speed of impeller are transferred to a computer through an A/D converter with the sampling frequency of 10kHz. The casing was made of transparent acryl resin for visual observation. Pictures were taken by a high-speed camera with the frame rate of 1000 flame/sec.

Received February 24 2014; accepted for publication April 30 2014: Paper number O14016S
Corresponding author: Donghyuk Kang, Assistant professor, kang@me.aoyamc.jp

This paper was presented at 12th Asian International Conference on Fluid Machinery (AICFM), September 25-27 2013, Jogyakarta, Indonesia

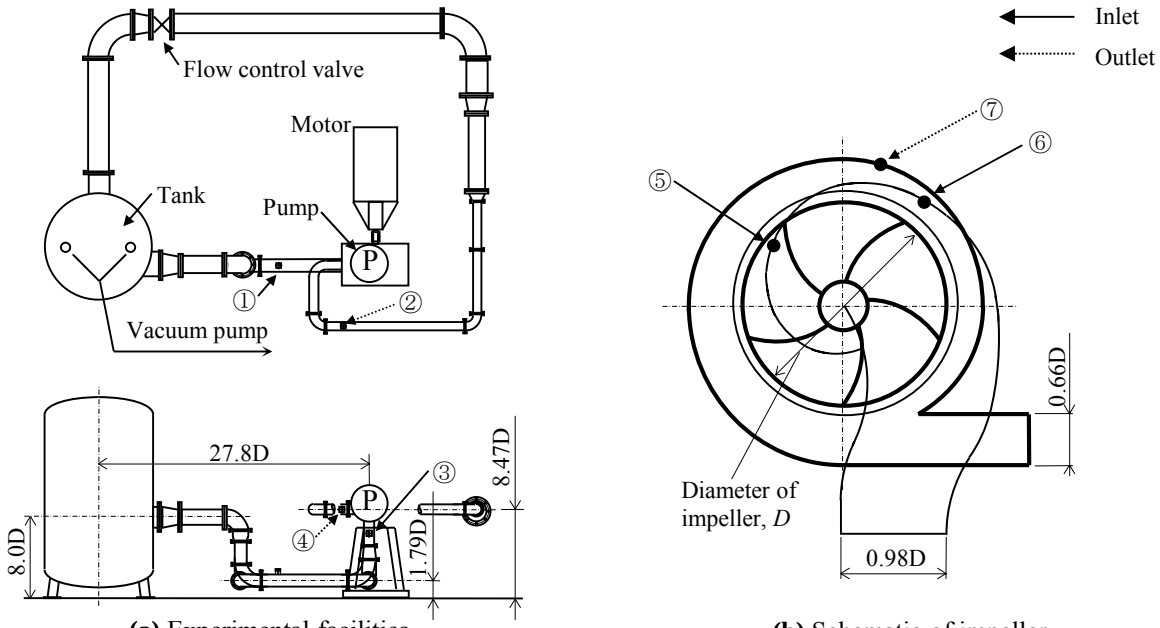

(a) Experimental facilities **(b)** Schematic of impeller

Fig.1 Experimental facilities and schematic of impeller

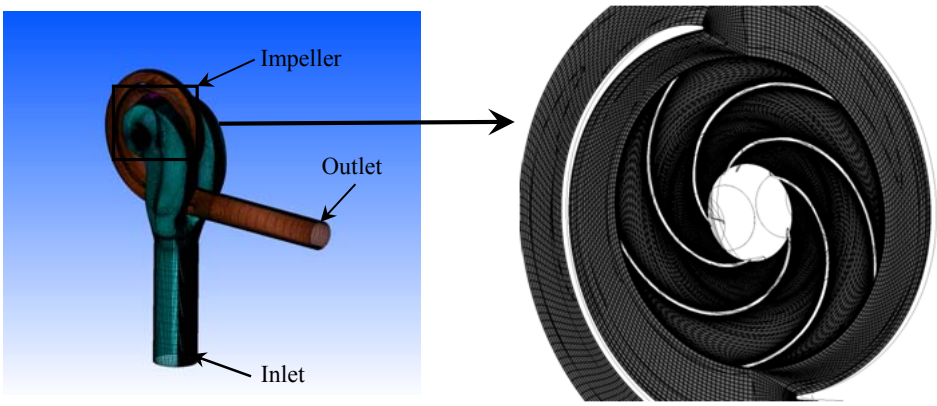

(a) Computational domain **(b)** Mesh for impeller

Fig. 2 Computational domain and mesh for impeller

2.2 Computational Method

A commercial software package, ANSYS-CFX 14.0 was used for the CFD of the cavitating flow of the double-suction centrifugal pump. Three dimensional Reynolds averaged Navier-Stokes (RANS) equations are solved by the finite volume method with the structured grid. Figure 2 shows the computational domain and the mesh for the impeller used in the present study. The number of computational cells of the impeller, the inlet pipe and the outlet pipe are about 2,260,000, 1,220,000 and 380,000, respectively. The cavitation model adapted in ANSYS-CFX14.0 is based on the homogeneous multiphase flow framework of the CFD solver taking into account the dynamic of cavitation bubble by solving a simplified Rayleigh-Plesset equation. This effect is taken into account by adding a special source term into the continuity equation. The k-ε turbulence model was used. The working fluids were the water and its vapor. The total pressure and the mass flow rate were specified at the inlet and outlet boundaries, respectively. As a first step, the steady CFD for the cavitating flow of the double-suction centrifugal pump were carried out. The steady CFD results were used for the initial values of the unsteady CFD. For the unsteady CFD, the time step is 1/100 of a revolution of the impeller and the second order schemes in space and time were used. All calculations were carried out until the pressure and the velocity for all measurement points becomes periodic.

3. Results and Discussions

3.1 Performance Curve

Figure 3 shows the noncavitating performance curves obtained from the experiment and the CFD results. The total pressure coefficient ψ is defined as $(p_{4t}\text{-}p_{3t})/(\rho U^2/2)$. Here, p_{3t} is the inlet total pressure at the suction pipe ③ and p_{4t} is the outlet total pressure at the discharge pipe ④. The gradient of performance curve of CFD is slightly lower than that of experiment for low flow rates. At the best-efficiency flow coefficient ϕ=0.0642, the CFD result agrees well with the experimental result.

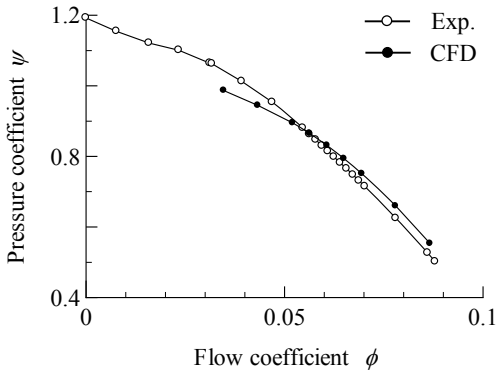

Fig.3 Performance curve, obtained from the experiment and CFD results

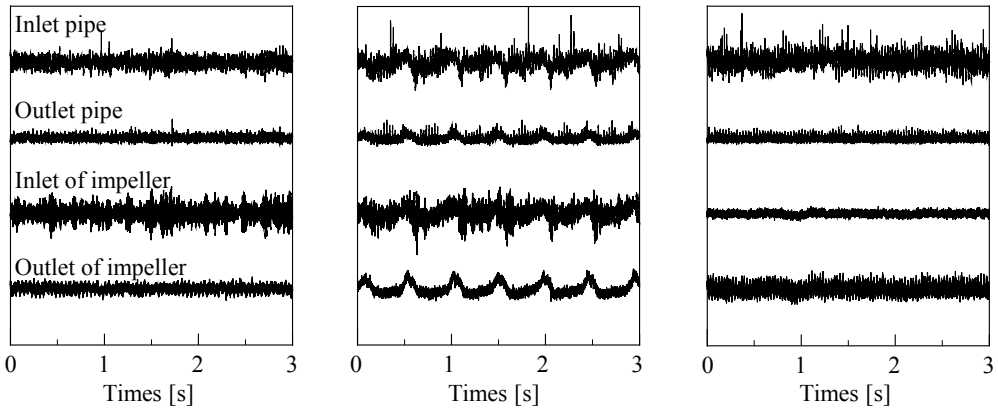

(a) σ=0.0431 **(b)** σ=0.0274 **(c)** σ=0.0214

Fig.4 Pressure oscillations at ϕ=0.0449, obtained from the experiment

3.2 Time Histories for Pressure Oscillations

Figure 4 shows the time histories for the pressure oscillations at ϕ=0.0449 for the various cavitation numbers. The pressures at the inlet and the outlet of the impeller were measured at ⑤ and ⑦ shown in Fig.1, respectively. At σ=0.0431, the significant oscillating pressure at the inlet pipe and the inlet of the impeller are observed, as shown in Fig.4(a). This may be caused by cavitation formed upstream of the impeller. At σ=0.0274, for all measurement points, the oscillating pressure with about 2Hz are observed, as shown in Fig. 4(b). This is due to the inertia force caused by the oscillating cavitation. This phenomenon is similar to cavitation surge with the flow and pressure oscillations. With further decreased cavitation number from σ=0.0274, it is confirmed that the periodic oscillating pressures disappear from all measurement points, as shown in Fig. 4(c).

3.3 Fast Fourier Transform (FFT) Analysis

Figure 5 shows the spectra of the pressure oscillation at the inlet of the impeller. The horizontal and vertical axes show the dimensionless frequency f^* normalized by the rotational frequency of the impeller f_n and the amplitude of the pressure oscillation $\Delta\psi=\Delta p/(\rho U^2/2)$, respectively. The depth axis indicates the cavitation number σ.

At ϕ=0.0244 and σ=0.2112, the dimensionless frequency component f^*=1.2 is decreased with the reduction of cavitation number. We confirmed that the phase difference between the pressures at ⑤, ⑥ installed with the circumferential interval of 90 degrees as shown in Fig.1(b), is approximately zero. Thus, this phenomenon can be considered to be a surge-type instability without cavitation, which is named *I*. In the range of *I*, serious vibration and noise were not observed. In the future, further investigations for the phenomenon *I* are needed.

At ϕ=0.0244 and in 0.0369<σ<0.0948, the frequency components higher than the rotational frequency of the impeller are observed. Consider the interaction of rotating cavitation with the impeller, in the assumption that rotating cavitation occurs upstream of impeller. We represent the frequency component of the pressure oscillation caused by the interaction of rotating cavitation with the impeller by [6]

$$f^* = nR\left(1 - f_c^*\right) + mf_c^* \tag{1}$$

Here, m and n are the number of order in θ and t, respectively. f_c^*=1.13 is the frequency of rotating cavitation determined by considering the frequency components in the relative frame evaluated from the unsteady CFD results. R is the number of blade. Table 1 shows the dimensionless frequencies calculated by Eq.(1) for various constants m and n. At ϕ=0.0449 and σ=0.0431, the

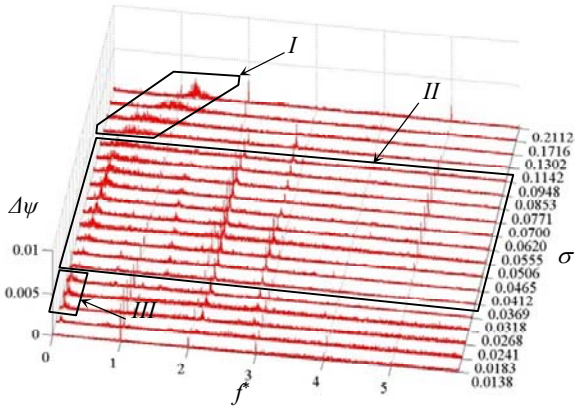

(a) ϕ =0.0244

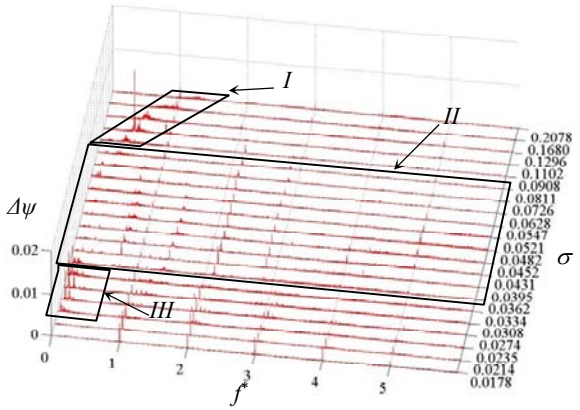

(b) ϕ=0.0449

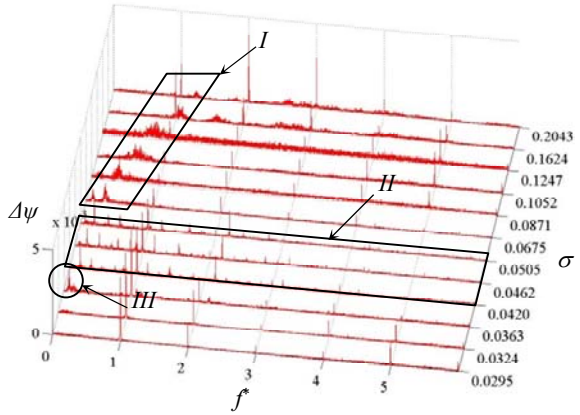

(c) ϕ=0.0642

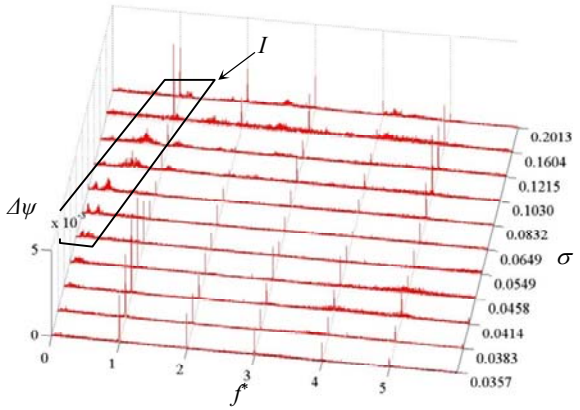

(d) ϕ=0.0731

Fig.5 Spectra of inlet pressure fluctuations for various flow coefficients, obtained from the experiment

Table 1 Dimensionless frequencies calculated for various constants *m*,*n*

	m =-2	*m* =-1	*m* =0	*m* =1	*m* =2
n =-4	0.57	1.71	2.85	3.99	5.14
n =-3	-0.15	1.00	2.14	3.28	4.42
n =-2	-0.86	0.28	1.43	2.57	3.71
n =-1	-1.57	-0.43	0.71	1.86	3.00
n =0	-2.29	-1.14	0.00	1.14	2.29
n =1	-3.00	-1.86	-0.71	0.43	1.57
n =2	-3.71	-2.57	-1.43	-0.28	0.86
n =3	-4.42	-3.28	-2.14	-1.00	0.15

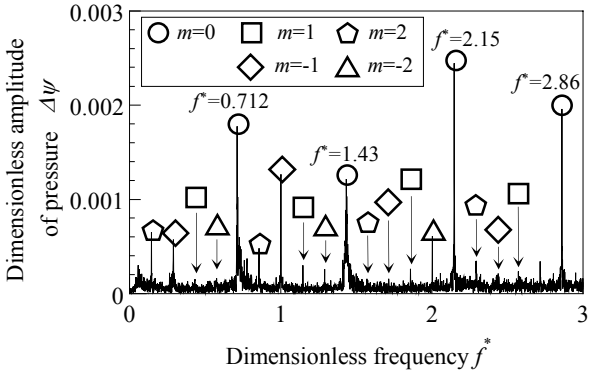

Fig. 6 Spectra of inlet pressure fluctuations at σ=0.0431,obtained from the experiment

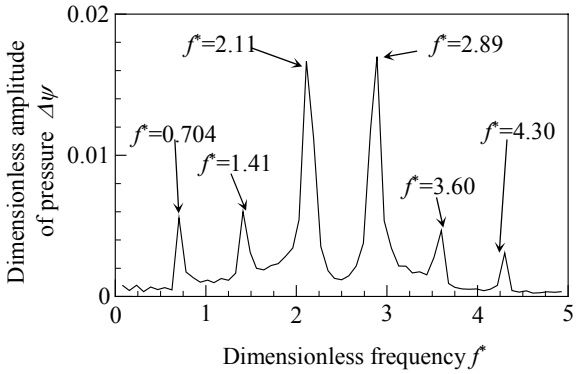

(a) σ=0.0532

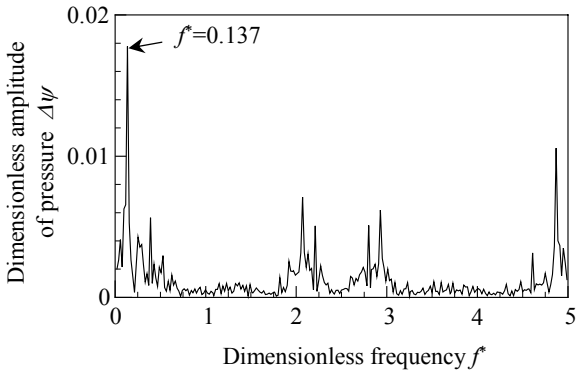

(b) σ=0.302

Fig. 7 Spectra of impeller pressure fluctuations at ϕ=0.0562, obtained from the CFD results

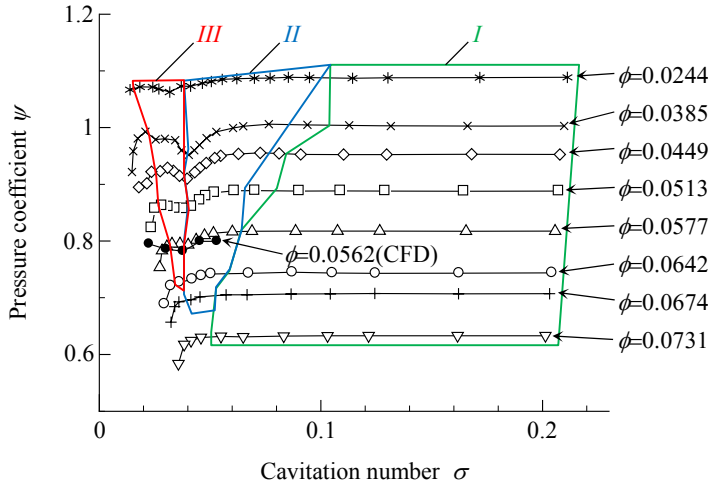

Fig. 8 Suction Performance curve, obtained from the experiment

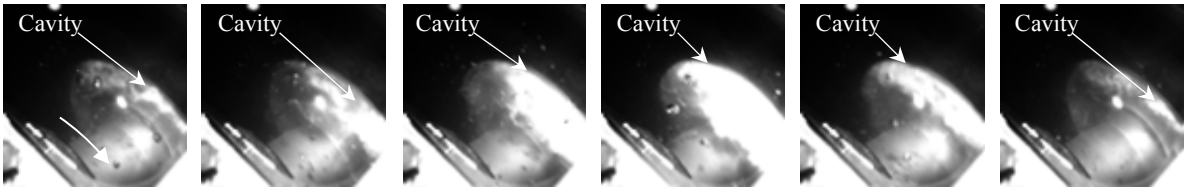

(a) t=0 **(b)** t=2T **(c)** t=4T **(d)** t=6T **(e)** t=8T **(f)** t=10T

Fig. 9 Pictures of cavities at ϕ=0.0449 and σ=0.0337, obtained from the experiment

spectrum of the pressure oscillation at the inlet of the impeller are shown in Fig.6. The symbols show the dimensionless frequencies shown by the gray background pattern of Table 1 for various m. Although not perfect, the frequencies calculated by Eq.(1) are in agreement with the experimental results. Therefore, we suppose that rotating cavitation occurs and it causes the pressure oscillation due to the interaction with the impeller. In this study, this phenomenon considered to be rotating cavitation is named *II*.

At ϕ=0.0244 and σ=0.0318, the low frequency component about f^*=0.1 is clearly observed with disappearing the frequency components due to the interaction of rotating cavitation with the impeller. The approximate zero phase difference between the pressures installed with the circumferential interval of 90 degrees was observed. Since the frequency component with the zero phase difference appears at the low cavitation number, this can be considered to be cavitation surge. In the present study, cavitation surge is named *III*.*I*, *II* and *III* are also confirmed in other flow coefficients.

Figure 7 shows the spectrum of the pressure oscillation of the inlet of the impeller at ϕ=0.0562 and σ=0.0532 and σ=0.0302, obtained from the CFD results. At σ=0.0532 where rotating cavitation occurs, the frequency components higher than the rotational frequency of the impeller are observed, as shown in Fig.7(a). The peaked frequency components are quite similar to the experimental results shown in Fig.6. At σ=0.0302 where cavitation surge occurs, the low frequency component with 0.137 is found as shown in Fig.7(b). These results suggest that the frequency components due to rotating cavitation and cavitation surge are mainly caused by the blade surface cavitation. In the CFD, cavitation surge occurs at the cavitation number lower than the cavitation number of rotating cavitation, identical to the experimental results.

3.4 Suction Performance Curves with Cavitation Instability Map

Figure 8 shows the suction performance curves with the cavitation instability map, obtained from the experiment and CFD results. The open symbols show the experimental results and the closed symbol shows the CFD results. The green, blue and red indicate *I*, *II* and *III*, respectively. The horizontal and vertical axes show the cavitation number σ and the total pressure coefficient ψ, respectively. The surge type instability *I* is observed in all flow rates and its occurrence region is widened with the increase of the flow coefficient. *II* due to the interaction of rotating cavitation with the impeller is observed in ϕ<0.0674 and its occurrence region is widened with the decrease of the flow coefficient. We observe the pressure degradation or rise at the cavitation number higher than the breakdown cavitation number. It was reported that the pressure degradation or rise of a cavitating pump is caused by the change of the pressure loss due to the unsteady cavitating flow [7]. Its mechanism, however, is not clearly clarified yet. It is interesting that the negative gradient of the suction performance curve is observed in the occurrence region of cavitation surge. Kang et al.[8] reported that the negative gradient of the suction performance curve causes cavitation surge.

3.5 Cavity Shape

Figure 9 shows the pictures of the clearance cavitation taken by a high-speed camera with the two periods of rotational impeller, at ϕ=0.0449 and σ=0.0337 where cavitation surge occurs. The clearance cavitation shown in Fig.9 occurs due to the shear layer caused by the main stream flow and the jet flow induced from the clearance between the rotor and the casing. Unfortunately, we could not observe the blade surface cavitation since the clearance cavitation obstruct our view. However, the

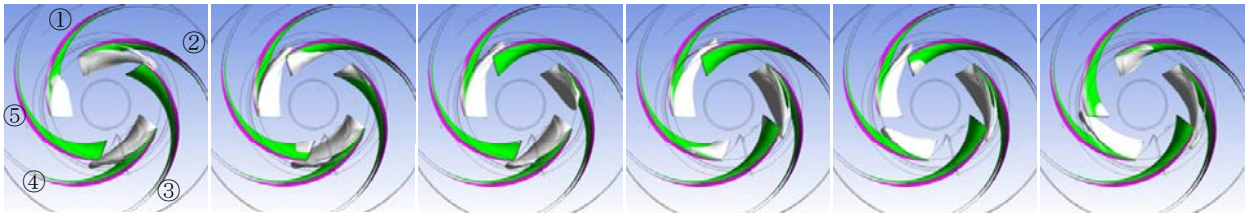

(a) t=0 **(b)** t=0.8T **(c)** t=1.6T **(d)** t=2.4T **(e)** t=3.2T **(f)** t=4.0T

Fig. 10 Cavity shapes at ϕ=0.0562 and σ=0.0532, obtained from the CFD results

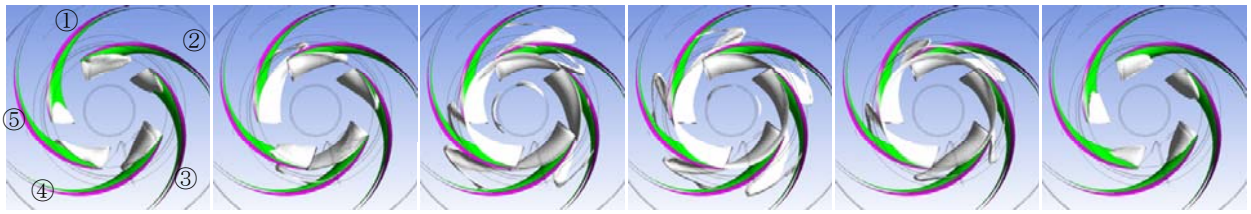

(a) t=0 **(b)** t=1.6T **(c)** t=3.2T **(d)** t=4.8T **(e)** t=6.4T **(f)** t=8.0T

Fig. 11 Cavity shapes at ϕ=0.0562 and σ=0.0532, obtained from the CFD results

significant oscillating clearance cavitation with the period of 10T (f^*=0.1) corresponding to the frequency of cavitation surge is observed.

Figure 10 shows a cavity shapes at ϕ=0.0562 and σ=0.0532 where *II* occurs. In the CFD, only the blade surface cavitation was simulated because the mesh for the clearance flow was not combined. The cavity was shown by a plane with the void fraction α=0.01. The propagation of the cavity is explained follows. We focus on the growth of the cavity of Blade ①. When the cavity of Blade ① is extended downstream and interacts with the leading edge of Blade ②, the cavity of Blade ② becomes small since the disturbance velocity at the cavity trailing edge causes the decrease of incidence angle to the next blade. The cavity of Blade ③ is extended downstream because the interaction of the cavity of Blade ② with the leading edge of Blade ③ is decreased, as shown in Fig.10(c). When the cavity of Blade ③ starts to interact with the leading edge of Blade ④, the cavity of Blade ④ is decreased, as shown in Fig.10(e). Therefore, the cavity rotates with interacting to the leading edge of next blade. This tendency is similar to the mechanism of the propagation of rotating cavitation observed in the axial pump [9].

Figure 11 shows cavity shapes at ϕ=0.0562, σ=0.0302 where cavitation surge occurs. The propagation of cavity is explained as follows. When the cavity of Blade ① is extended downstream, the cavity of Blade ② is not significantly decreased different from rotating cavitation shown in Fig.10(b). The cavity of Blade ① is further extended downstream with interacting the leading edge of Blade ②, as shown in Fig.11(b)~(c). The cavity of Blade ② develops downstream with interacting the leading edge of Blade ③, as shown in Fig.11(c)~(d). When extending downstream of throat, all cavities decrease at the same time, as shown in Fig.11 (d)~(e). The period of oscillating cavitation is about 8T, similar to the experimental result of 10T.

Conclusions

The experiment and CFD were performed to identify cavitation instabilities in the double-suction centrifugal pump. The cavitation instabilities in the tested pump were classified into three types of instabilities. The first one, in a range of cavitation numbers higher than the breakdown cavitation number, is cavitation surge with the violent pressure oscillation. The second one, in a range of cavitation number higher than the cavitation number of cavitation surge, is considered to be rotating cavitation and causes the pressure oscillation due to the interaction of rotating cavitation with the impeller. Last one, in a range of cavitation number higher than the cavitation number of rotating cavitation, is to be a surge type instability.

Acknowledgments

The authors would like thank Prof. Tsujimoto of Osaka University who gave useful suggestions to make this study more valuable. This study was made under the support of Grant-in-Aid of EBARA Corporation.

Nomenclature

D	Diameter of inducer [m]	α	Void Fraction[-]
f^*	Dimensionless frequency of pressure oscillation [-]	θ	Circumferential location [degree]
f_c^*	Dimensionless frequency of rotating cavitation [-]	ρ	Density of water [kg/m^3]
f_n	Rotational frequency of the impeller [Hz]	σ	Cavitation number =$(p_3-p_v)/(\rho U^2/2)$ [-]
m	Number of order in θ	ϕ	Flow coefficient = v/U [-]
n	Number of order in t	ψ	Pressure coefficient =$(p_{4t}-p_{3t})/(\rho U^2/2)$ [-]
p_3	Static pressure at the inlet [Pa]	$\Delta\psi$	Fluctuating pressure coefficient =$\Delta p/(\rho U^2/2)$ [-]
p_{3t}	Total pressure at the suction pipe [Pa]		
p_{4t}	Total pressure at the discharged pipe [Pa]		
p_v	Vapor pressure [Pa]		
Δp	Amplitude of pressure oscillation[Pa]		
t	Time [s]		
U	Tip speed of impeller [m/s]		
v	Mean axial velocity at the suction pipe③ [m/s]		

References

[1] Acosta, A. J.,1958, "An Experimental Study of Cavitating Inducers," Proceeding of the Second Symposium on Naval Hydrodynamics, ONR/AVR-38, pp. 533-557.

[2] Tsujimoto, Y., Yoshida, Y., Maekawa, Y., Watanabe, S. and Hashimoto, T., 1997, "Observations of Oscillating Cavitation of an Inducer," J Fluid Eng-Trans ASME, 119, pp. 775-781.

[3] Young,W.E., 1972, "Study of Cavitating Inducer Instabilities, Final Report," NASA-CR-123939.

[4] Yamamoto, K., 1990, "Instability in a Cavitating Centrifugal Pump (1st Report, Classification of Instability Phenomena & Vibration Characteristics)," Trans. JSME (in Japanese), Ser.B, Vol. 56, No. 523, pp. 82-89.

[5] Yamamoto, K., 1990, "Instability in a Cavitating Centrifugal Pump (2st Report, Delivery of Mechanical Energy during Oscillation)," Trans. JSME (in Japanese), Ser.B, Vol. 56, No. 523, pp. 90-96.

[6] Kang, D.,Arimoto, Y., Yonezawa, K., Horiguchi, H., Kawata, Y., Hah, C. and Tsujimoto, Y., 2010, "Suppression of Cavitation Instabilities in an Inducer by Circumferential Groove and Explanation of Higher Frequency Component," International Journal of Fluid Machinery and Systems, Vol. 3, No. 2, pp. 137-149.

[7] Ng.S.L. and Brennen, C.E., 1978, "Experiments on the dynamic behavior of cavitating pumps," J Fluid Eng-Trans ASME, 100, pp. 166-176.

[8] Kang, D. and Yokota, K., 2014, "Analytical Study of Cavitation Surge in Hydraulic system," J Fluid Eng-Trans ASME, 136, pp. 101103-1-101113-10.

[9] Kang, D., Yonezawa, K., Horiguchi, H., Kawata, Y., and Tsujimoto, Y., 2009, "Cause of Cavitation Instabilities in Three-Dimensional Inducer," International Journal of Fluid Machinery and Systems, Vol. 2, No. 3, pp. 206-214.